JAAS

Accepted Manuscript

This is an *Accepted Manuscript*, which has been through the Royal Society of Chemistry peer review process and has been accepted for publication.

Accepted Manuscripts are published online shortly after acceptance, before technical editing, formatting and proof reading. Using this free service, authors can make their results available to the community, in citable form, before we publish the edited article. We will replace this *Accepted Manuscript* with the edited and formatted *Advance Article* as soon as it is available.

You can find more information about *Accepted Manuscripts* in the Information for Authors.

Please note that technical editing may introduce minor changes to the text and/or graphics, which may alter content. The journal's standard Terms & Conditions and the Ethical guidelines still apply. In no event shall the Royal Society of Chemistry be held responsible for any errors or omissions in this *Accepted Manuscript* or any consequences arising from the use of any information it contains.

ROYAL SOCIETY OF CHEMISTRY

www.rsc.org/jaas

ARTICLE TYPE www. rsc.org/xxxxxx | XXXXXXXX

Enhancement of Intensity in Microwave-Assisted Laser-Induced Breakdown Spectroscopy for Remote Analysis of Nuclear Fuel Recycling †

Motonobu Tampo *, Masabumi Miyabe, Katsuaki Akaoka, Masaki Oba, Hironori Ohba, Yoichiro Maruyama, and Ikuo Wakaida

Received Xth XXXXXXXXXX 2013, Accepted Xth XXXXXXXXX 20XX
First published on the web Xth XXXXXXXXXX 200X
DOI: 10.1039/b000000x

An enhancement of emission intensity from laser ablation plume, obtained by coupling a pulsed microwave using a simple wire antenna, is demonstrated to compensate the sensitivity reduction of higher resolution spectrometer that is required for nuclear fuel analysis. A gadolinium oxide sample was irradiated with 2.45 GHz, 250 W microwave pulse, passed through a loop antenna. As a result, up to 50-fold enhancement of emission signal was achieved for gadolinium ions. The enhancement enabled to measure the mass concentration of europium per gadolinium, ranging from 5 % to 100 ppm, and based on the extrapolation of calibration curve the detection limit for microwave-assisted laser induced breakdown spectroscopy (MA-LIBS) was estimated to be 40 ppm. This offers a flexible and compact system of MA-LIBS for nuclear fuel analysis.

1 Introduction

Next generation fuels are attracting an increased attention of researchers working in the field of nuclear fuel cycle. These fuels are expected to contain not only uranium and plutonium, but also trans-uranium elements and radioactive fission products. Introduction of new fuels is advantageous, for the following reasons: (i) it may simplify the reprocessing process, (ii) it may reduce the environmental burden by long-lived fission products, (iii) it may contribute to a sustainable use of nuclear fuel resources, and (iv) it may contribute to a higher resistance to nuclear proliferation. Laser-induced breakdown spectroscopy (LIBS) is likely to become a quick and convenient remote analysis tool for monitoring and tracing a mass flow of U and Pu in the fuel production process under strong radiation fields[1,2]. Application of LIBS to heavier atoms such as U, Pu and trans-uranium elements requires higher resolution power (<0.0004 nm) of LIBS spectrometer in order to identify each emission line separately. Such spectrometer, however, is in general less sensitive, and thus requires a more intense source of emission.

Several approaches to enhance the emission signal have been suggested, such as a double pulse LIBS[3–7], a laser induced fluorescence LIBS[8–14], a resonant LIBS[15–20], a spark-discharge LIBS[21–24], and a glow discharge LIBS[25–27]. These methods allow inputting additional electromagnetic energy into the ablation plume by using secondary energy sources that employ an additional laser or spark discharged plugs. Another candidate to serve as a secondary energy source is the microwave device. Because the microwave can effectively transfer the electromagnetic energy into plasma, and because the microwave device is cheaper than the additional laser device, the use of a microwave to create an intense emission has been suggested and demonstrated in several reports[28–31]. This method, known as the microwave-assisted LIBS (MA-LIBS), has succeeded in sustaining a plasma emission for few milliseconds, resulting in signal enhancement by temporal integration. In these reports, the microwave is coupled to the ablation plume by using wave transfer tube and a cavity well covering a sample target. However, during the operation of nuclear fuel recycling process all equipment should be compact and simple in order to reduce the amount of nuclear pollution as well as the volume and the area that are affected by it. In addition, whereas a quick exchange mechanism for sample targets is required in LIBS for treating many samples, the use of a microwave cavity makes difficult to design the mechanism. To overcome these difficulties, we have studied MA-LIBS using a small wire antenna which can be close to the sample surface by a simple translational mechanism.

In the present paper, MA-LIBS using antenna is described as a first experimental setup that yields enhanced signal and improved stability as compared with the results that are obtained by using the conventional LIBS.

* *Japan Atomic Energy Agency (JAEA), Nuclear science and engineering Directorate,319-1197, Shirakata Tokai-mura, Naka-gun, Ibaraki, Japan. Fax: XX XXXX XXXX; Tel: +81-(0)29-282-6008;E-mail: mtampo@post.kek.jp*

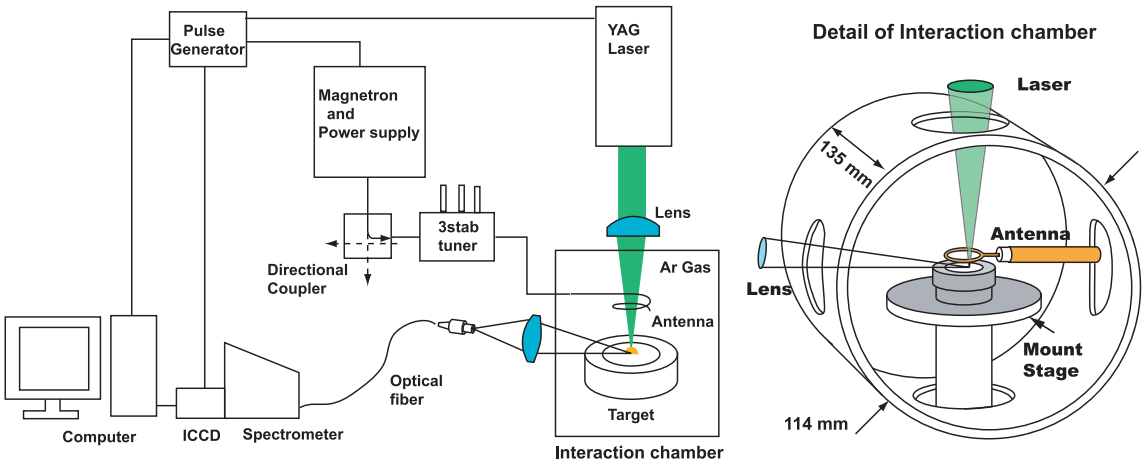

Fig. 1 Schematic drawings of the experimental setup. The sample target mounted on the stage (diameter of 70 mm) is positioned in the center of a cylindrical chamber with 3 lateral window ports and 2 vertical ports. The lateral windows with a diameter of 50 mm, placed on the cylindrical side, are used to observe the emission spectra and the input microwave. In order to shield the leakage of the microwave all windows are covered by the metal mesh with 2 mm spacing and 15 μm-diameter gold wire.

2 Experimental

Experimental setup is depicted in Fig. 1. A target sample consisted of gadolinium oxide pellets with 1 mm thickness and 10 mm in diameter. These were made by compressing gadolinium oxide powder of 1 g by the pressure of 1.5 MPa, and then sintering at 1400 °C for 5 hours. The target sample was placed on a mount stage in an interaction chamber and was affixed to the stage by screwing a metal covering cap (25 mm in diameter) that had an opening hole of 9 mm in diameter. The mount stage was rotated at a speed of 0.3 rad/sec during the experiment, in order to avoid the crater effect. The Ar gas (purity 99.99 %) was used as the ambient gas. The chamber was evacuated by a rotary pump and flushed with the Ar gas several times. The measurements were made under conditions of continuous pumping and gas flow at a constant pressure of 0.6 kPa. The laser pulse that had the energy of 5 mJ, pulse duration of 5 ns and wavelength of 532 nm, and that was obtained from the Nd:YAG laser (Brilliant B: Quantel), was focused on the target sample by a lens that had the focal length of 250 mm. The diameter of focal spot was evaluated to be 200 μm, based on the optical microscope observations for the crater on the sample. A typical intensity of the laser at the spot was 3.2×10^9 W/cm^2. Emission from the produced ablation plume was collected by a lens (150 mm in diameter, focal length of 200 mm) and was transported into an optical fiber (core diameter of 400 μm). The collection lens was placed at a distance of 200 mm from the focal spot on the target. The fiber head was placed at a distance of 250 mm from the collection lens. The collected emission was measured by using the Echelle spectrometer with ICCD (ARYELLE 400: LTB Lasertechnik Berlin GmbH) that had a spectral resolution of 0.0004 nm.

2.1 Microwave input

To input the microwave pulse into the ablation plume, we used a 2.45 GHz magnetron with an output power of 250 W (MG0500D, Muegge). Since the magnetron used in this study takes about 10 μs until the output reaches to the constant power of 250 W, the microwave pulse irradiation was started from 10 μs before each laser shot. The pulse width was set to be 300 μs, which was controlled by inputting gate signal from the delay generator (DG535: Stanford Research Systems) into the magnetron generator. The microwave pulse was transported by a 50 Ohm coaxial cable (S 10162 B-11: HUBER+SHUNER) and delivered a directional coupler and a three-stab tuner. From the tuner, the cable was changed into a 1 m semi-rigid cable (RG402U), with its outer diameter being 3 mm, for better flexibility in delivering the microwave pulse. The semi-rigid cable was laterally inserted into the chamber using an injector with three-dimensional moving stage, and terminated with a connector for attaching various antennas with connector. The antenna was made from the semi-rigid cable with a core metal wire of $\sim$1 mm diameter by removing the metal sheath and the PTFE layer. The antenna consisted of the wire with a length of $\lambda/4$ ($\sim$30.6 mm, λ: microwave wavelength) and a 40 mm long coaxial cable with connector. The antenna was loop-shaped with a diameter of 9 mm in order to generate the electromagnetic field to surround the ablation plume. The electro-magnetic field is theoretically non-uniform, which are approximately proportional to the distance from the center of the loop[32]. The antenna was vertically placed at the height of 1.5 mm from the sample surface. Also,

the focal spot of the laser was laterally placed at the center of the loop. Microwave power was tuned by the three-stab tuner to yield maximal subtraction between input and reflected wave signals on the directional coupler. After the tuning, the maximal subtraction of 80 % was achieved.

3 Results and Discussion

3.1 Excitation temperature and its temporal variation

Emission spectra in the wavelength range of 250–1100 nm were observed by accumulating the data over an interval of 5 μs at delays of 2, 12, 62, 112, 162, 212, and 262 μs after the laser firing, both for the cases with and without the microwave. Among these spectra, 19 and 23 line spectra were assigned to be the emissions of Gd(I) and Gd(II) with upper energy levels ranging from 2.24 eV to 4.32 eV for Gd(I) and from 3.18 eV to 4.32 eV for Gd(II)[33]. Temporal variations of Boltzmann plots were evaluated for Gd(II) and Gd(I) by using the observed line intensities, the relevant upper level energies, and the transition probabilities, as is shown in Figs. 2(a) and 2(b). In Fig. 2(a), the Boltzmann plots of Gd(II) emission intensities were shown up to 12 μs for the laser-only case and up to 212 μs for the case of microwave coupling. In the laser-only case, the emission intensities rapidly decreased below the detection limit at a delay of $>$10 μs. In the case of microwave coupling, the emission intensities slowly decreased below the detection limit at a delay of $>$260 μs. By fitting the Boltzmann distribution function: $N=N_0 \cdot \exp(-x/T)$ (where x is the upper level energy and T is the excitation temperature), the temperatures for Gd(I) and Gd(II) were evaluated in the laser-only and microwave coupling cases.

Figure 3 shows the evaluated temperatures as a function of the delay time from laser firing. This is likely to be the first reported temperature evaluation for a microwave-coupled ablation plume. The error bar was estimated from the deviation of each data point from the fitted curve based on the error propagation theory. In the case when only the laser was used, the excitation temperature was observed to decrease monotonically following the ablation. A similar behavior has been reported by several researchers[34–36] and it was attributed to the plume's expansion cooling that was mitigated by heat that is released through electron-ion recombination and shockwave-induced plume compression[37]. On the contrary, in the microwave coupling case, the temperature was found to be increasing with time. Furthermore, as Fig. 3 shows, whereas the difference in the temperature between the microwave coupling and the laser-only cases is insignificant for the delay of around 2 μs, the difference becomes apparent for the $>$12 μs delay especially for Gd ion. This suggests that an effective microwave energy transfer into the ablation plume starts from the delay of $\sim$10 μs. A possible explanation for such delaying

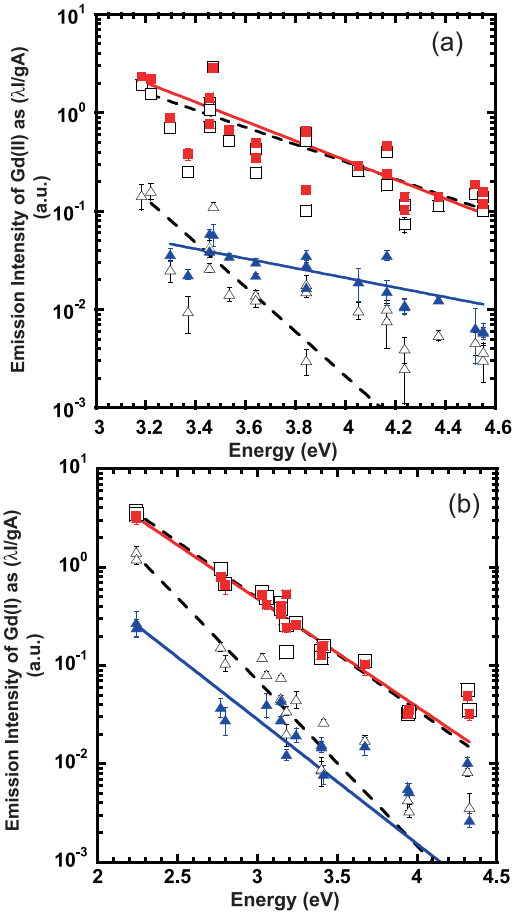

Fig. 2 Boltzmann plots of (a) Gd(II) and (b) Gd(I) at different time delays, obtained from the spectral peaks of Gd emissions from laser ablation plume with (filled symbols) and without (open symbols) microwave coupling. Open square and triangle (laser only) are data for the timing of 2 and 12 μs delayed from laser shot. Filled square and triangle (microwave coupling) in plots (a) are data for the delay of 2 and 212 μs and those in plots (b) are data for the delay of 2 and 60 μs. The microwave pulse irradiation with 300 μs duration was started from 10 μs before each laser shot.

of the microwave coupling effect is that immediately following the laser firing the plasma density is very high, so that the microwave radiation cannot interact with the ablation plume except at the outer edge of the plume. The critical density at which a microwave with 2.45 GHz is cut off is estimated to be 7×10^{10} cm^{-3}. Because the density of the plasma immediately following the laser firing could be higher than 10^{17} cm^{-3} and it decreases rapidly with the expanding plasma and ongoing electron-ion recombination, there exists some temporal delay until the density of plasma becomes lower than the cutoff density, below which the microwave is able to interact with the ablation plume.

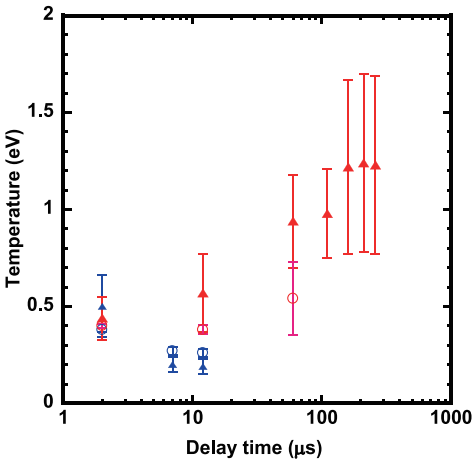

Fig. 3 Temporal evolution of excitation temperature from Boltzmann plots in Fig. 2. The microwave coupling cases are indicated with red filled triangles (Gd(II)) and open circles (Gd(I)) whereas laser only cases are indicated with blue filled triangles (Gd(II)) and open circles (Gd(I)). The horizontal axis represents delay time from laser firing.

3.2 Temporal evolution of emission intensity

As described in the previous section, the microwave coupling to the laser-induced plasma sustained the plasma emission of Gd ions and atoms for durations that were 26 times and 6 times longer compared to the laser-only case. The differences in the plasma lifetime between Gd(I) and Gd(II) can be seen in Fig. 4, which depicts the temporal evolution of the intensity of two emission lines: 1) 367.1205 nm for Gd(II), and 2) 371.7484 nm for Gd(I), as listed in Table 1. These lines were selected to compare the Gd(I) and Gd(II) populations with the upper energy levels around 3.4∼3.45 eV. The vertical scale of the plots in Fig. 4 is proportional to the population in the upper level, similar to the Boltzmann plots in Fig. 2. Regardless of the microwave coupling, the population of Gd ions was approximately 10 times larger than that of the atoms. In addition, it is noteworthy that the microwave coupling did not enhance the populations at a delay of 2 μs. The effect of microwave coupling is clearly dominant at times later than $\sim$ 10 μs following the laser firing. In addition, starting from the time of $\sim$10 μs the microwave power is absorbed more effectively by ions rather than by neutral atoms. One of the explanations for such highly effective microwave coupling to the ions is the difference between the spatial distributions of Gd(II) and Gd(I) in the ablation plume. Several reports, in which lanthanide elements were used, revealed that ions and atoms are distributed in the outer and inner parts of ablation plume, respectively[38]. Because the electromagnetic field of the microwave is generated from the loop antenna that surrounds the plume, the electromagnetic field first faces the outer part of the plume where ions are dominant. As a result, the microwave energy can be absorbed by the ions prior to the neutral atoms. Similar to the discussion in the previous section, delaying of the microwave effect is observed not only on the temperature but also on the population of excited states for ions and atoms.

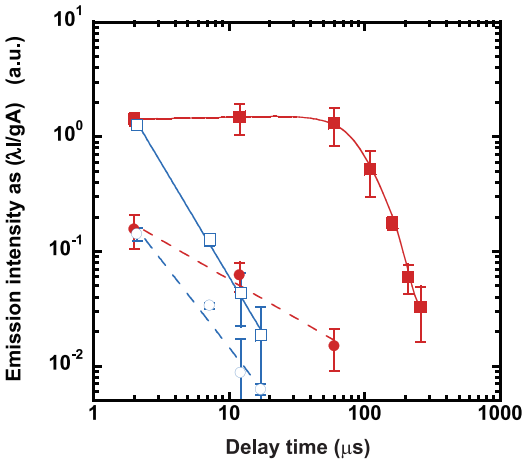

Fig. 4 Temporal evolution of emission intensities for 367.1205 nm Gd(II) (squares) and 371.7484 nm Gd(I) (circles), obtained with (filled red) and without (open blue) microwave coupling.The horizontal axis represents delay time from laser firing.

3.3 Spatial distribution of integrated emission intensity

By integrating the emission intensity over the interval of 350 μs, we have found the best positions in which the most intense signals of Gd(I) and Gd(II) can be obtained. Figure 5 shows the spatial distributions of the resultant integrated intensities with error bars corresponding to 3σ variances for the lines in Table 1. These were measured by varying the height of the fiber head collecting emission in steps of 1 mm, in the direction perpendicular to the target surface. This intensity means the time-integrated population in the upper level. For the case of microwave coupling, emissions of Gd(I) and Gd(II)

Table 1 Spectral lines used to compare Gd(I) and Gd(II) populations [33].

Wavelength (nm)	Upper level energy (cm^{-1} (eV))	Lower level energy (cm^{-1} (eV))	Transition probability (sec^{-1})	J upper	J lower	Species
371.7484	27425.245 (3.40053)	532.977 (0.066085)	$6.747 \cdot 10^7$	4	4	Gd(I)
367.1205	27864.534 (3.45499)	633.273 (0.078)	$1.928 \cdot 10^7$	5.5	4.5	Gd(II)

are distributed up to a height of ~9 mm, whereas for the laser-only case the integrated intensity rapidly decreases above a height of 5 mm. The highest enhancement of integrated intensity was obtained at a height of 3 mm for the microwave coupling case and at a height of 2 mm for the laser-only case. Thus, the experiments in Figs. 2 and 4 were performed using these height values. As a result, using the microwave coupling we achieved a 25-fold enhancement of Gd(II) intensity and a 5-fold enhancement of Gd(I) intensity. As is shown in Fig. 4, these gain differences are due to the differences in emission durations of Gd(II) and Gd(I).

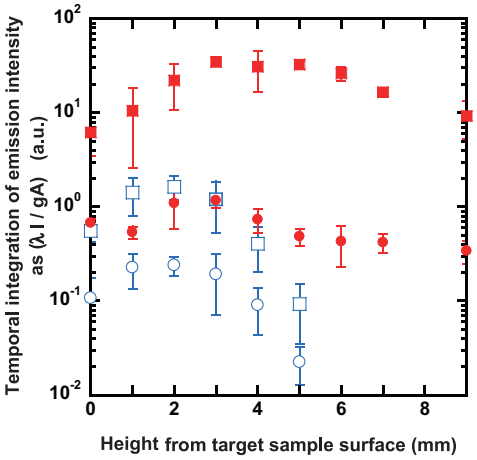

Fig. 5 Spatial distributions of temporally integrated intensities for 367.1205 nm Gd(II) (squares) and 371.7484 nm Gd(I) (circles), with (filled red) and without (open blue) microwave coupling.

3.4 Enhancement of integrated intensity by microwave

To evaluate the extent of intensity enhancement for a wide range of wavelengths, we obtained temporal integrations of Boltzmann plots for Gd ions and atoms from the spectra that were measured with the 350 μs long exposure of ICCD camera from the 2 μs delay, as is shown in Figs. 6(a) and 6(b). In these figures the error bars denote the 3σ variance of the measured data points. Each curve corresponds to the temporal integration of time-dependent Boltzmann plots for Gd ions and atoms in Figs. 2(a) and 2(b). By fitting the Boltzmann distribution function to the curves in Fig. 6(a), the fitting coefficients of N_0 = 3146.9 and T=0.686 eV were obtained for the microwave coupling case, and N_0=1386.4 and T=0.472 eV for the laser-only case. Thus, the enhancement of intensity as a function of an upper level energy of x can be expressed as $2.2699 \cdot \exp(0.66871 \cdot x)$ by taking a fraction of the fitting curves for both cases. From this equation, it was found that, for Gd ions, the minimal enhancement with microwave coupling was 20-fold at 3.2 eV and the maximal enhancement was 50-fold at 4.5 eV.

Similarly, based on the Boltzmann plots of Gd atoms in Fig. 6(b), the fitting coefficients of N_0=905.02 and T=0.488 eV were obtained for the microwave coupling case, and the coefficients of N_0=958.1 and T=0.439 eV were obtained for the laser-only case. Thus, the enhancement of intensity for Gd atoms can be expressed as $0.9446 \cdot \exp(0.23093 \cdot x)$. From this equation, it was found that, for Gd atoms, the minimal enhancement was 1.6-fold at 2.3 eV and the maximal enhancement was 2.6-fold at 4.4 eV.

These results clearly show that the enhancement of intensity with microwave coupling increases with increasing upper level energy, both in the case of Gd atoms and in the case of Gd ions. Specifically, the enhancement of integrated intensity for Gd ions was ~2.5 times larger for upper levels around 4.5 eV than for the levels around 3 eV. This result is in qualitative agreement with the result that is shown in Fig. 3, in which the excitation temperature of Gd ions increases with increasing temporal delay. The 20-50-fold enhancement of the intensity of Gd ion emissions allows reducing the average number and/or compensating for the sensitivity reduction when super-high resolution spectrometers are used, as described in Introduction (Sec. 1).

3.5 Analytical performance of MA-LIBS

To confirm the availability of MA-LIBS using the wire antenna we have demonstrated the spectroscopic analysis of europium concentration that was mixed into the gadolinium samples. We prepared the samples by mixing Eu and Gd oxides with Eu mass concentrations of 100, 250, 500, 2500 ppm, 1.0 and 5.3 %. Fig. 7 shows the emission spectra measured with samples with three different Eu concentrations. The spectroscopic data for these peaks and the relevant energy levels are summarized in Table 2.

The spectra without the microwave coupling in Fig. 7(b) were measured by accumulating 100 shot signals with an ICCD gain of 250. On the other hand, the spectra with the

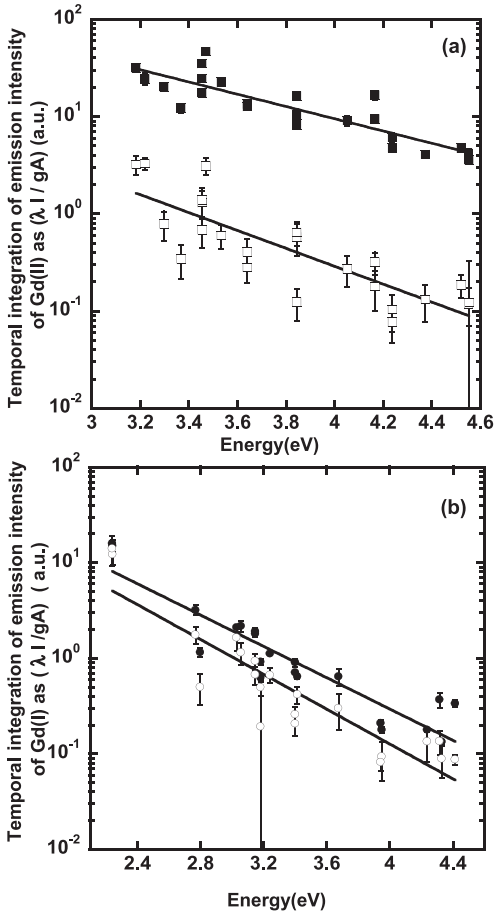

Fig. 6 Temporally integrated Boltzmann plots for (a) Gd(II) and (b) Gd(I), obtained from spectral intensity measured with 350 μs long exposure of an ICCD camera in spectrometer, with (black) and without (white) microwave coupling.

microwave coupling in Fig. 7(a) were obtained by accumulating 30 shots with an ICCD gain of 150, to avoid camera saturation. The actual ICCD gain for the laser-only case is 10 times higher than that for the microwave coupling case, which is calibrated by using a standard light source. As is shown in Fig. 7, the height of peak no. 2 (see Table 2) varies with mass concentration of Eu. However, in the laser-only case, peak no. 2 for Eu concentration of 500 ppm is likely to be hidden by other unknown peaks. On the other hand, in the microwave coupling case, peak no. 2 for this concentration can be clearly identified. Also, the reproducibility of the peak height with the microwave coupling is apparently higher than that without the microwave (for example, peaks nos. 3 and 4). This significant improvement of reproducibility can be also seen in smaller error bars of Boltzmann plots in Fig. 6.

Figure 8 shows the calibration curves that were evaluated from the emission intensity of peak no. 2, with and without

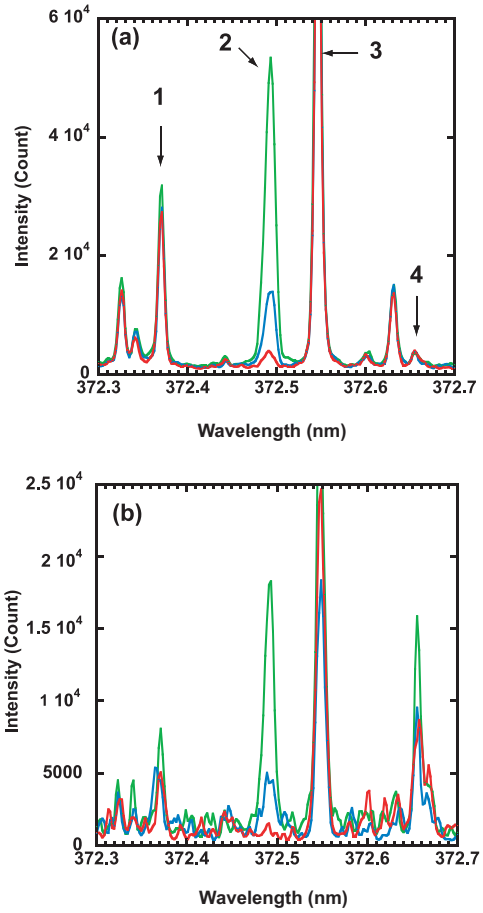

Fig. 7 Emission spectra for Gd and Eu mixed samples with Eu concentrations of 1% (Green), 2500 ppm (Blue), and 500 ppm (Red), measured with (a) and without (b) microwave coupling. Spectroscopic data for emission peaks of nos.1-4 are summarized in Table 2. Since the measurement conditions for both figures are different, a correction is needed to compare the emission intensities of both figures (see in text).

Table 2 Summary of spectral lines in Fig.7[33].

Peak No.	Wavelength (nm)	Upper level energy (cm^{-1} (eV))	Lower level energy (cm^{-1} (eV))	Transition probability (sec^{-1})	J upper	J lower	Species
1	372.3686	40773.207 (5.05574)	13925.734 (1.726687)	$6.747 \cdot 10^7$	6.5	6.5	Gd(II)
2	372.4931	26838.5 (3.327774)	0.0 (0.00000)	$1.928 \cdot 10^7$	4	4	Eu(II)
3	372.5469	36778.403 (4.560248)	9943.779 (1.232955)	$6.25 \cdot 10^7$	4.5	5.5	Gd(II)
4	372.6580	27041.751 (3.352976)	215.124 (0.026674)	$6.43 \cdot 10^6$	3	3	Gd(I)

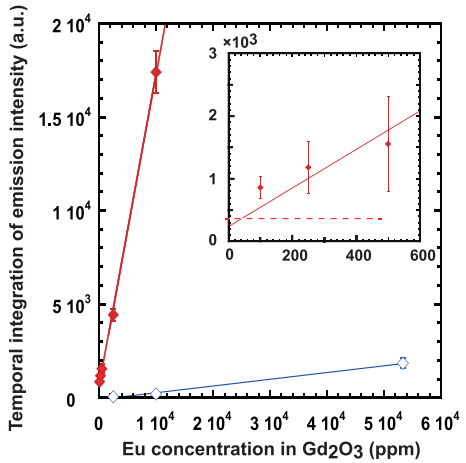

Fig. 8 Calibration curves of Eu mass concentration with (filled red) and without (open blue) microwave coupling. Inset shows an enlarged figure around the origin. A horizontal broken line indicates background level for MA-LIBS. From the interception between the broken line and the calibration curve the detection limit for MA-LIBS is roughly evaluated to be 40 ppm.

the microwave coupling. In this measurement, the emission signal was accumulated over 100 shots for the laser-only case and over 30 shots for the microwave coupling case. Moreover, the data for each concentration was obtained by averaging over 10 independent measurements. Considering the above described differences in shot numbers and in the ICCD gain, the emission intensities with and without the microwave coupling were corrected to ensure comparison in Fig. 8. The vertical axis means the time-integrated emission intensity.

As described in section2, in the present study we used a high resolution spectrometer; nevertheless line densities for Eu and Gd emission spectra were still high. Thus the emission intensity of peak no.2 is most likely to be biased by overlapping tails of many adjacent peaks. By measuring the bias intensities using a pure Gd pellet as a blank sample under the experimental conditions same as figure 8 and adding 3 $\sigma-$variances to the averaged intensities, the background levels for with and without microwave cases were determined to be 360 and 36. From these levels and calibration curves, the detection limits were roughly evaluated to be 40 ppm and 500 ppm for LIBS with and without microwave coupling, which ensured the approximately one-order improvement in detection limit for MA-LIBS. Microwave coupling provide also a good linearity over a wide range of Eu concentration with an accuracy better than the laser only case. Although this evaluation of calibration curve is preliminary attempt using simple antenna, we were able to demonstrate higher analytical performance of the MA-LIBS in comparison to a conventional LIBS.

4 Conclusions

Antenna-coupled MA-LIBS was studied to enhance the emission intensity in an attempt to solve the issue of sensitivity reduction in super-high resolution spectrometers, which are required for nuclear fuel analysis. The pulsed microwave input (2.45 GHz, 250 W, and 300 μs) through a wire loop antenna (diameter of 9 mm) has temporally sustained plasma emissions for a period of around 300 μs for Gd ions, a duration which is 10 times longer than the one that is obtained without microwave coupling. By integrating the temporal emission of Gd ions, we have achieved a 50-fold increase in emission intensity as compared to the laser-only case. Using mixed Eu and Gd samples, a good linearity of the calibration curve, a better reproducibility and a higher sensitivity were demonstrated with smaller shot accumulations for the MA-LIBS.

In the present study, we used a single-turn loop-antenna to ensure the improvement in analytical performance of LIBS using microwave irradiation. To fulfil this purpose we reported only the results of 9 mm antenna which gave the best performance among several antennas of 4-16 mm diameters in our preliminary study. Theoretically, the interaction between ablation plume developing perpendicular to the sample surface and microwave become more effective using a multi-turn helical antenna owing to the longer interaction time. Thus we have a plan to seek the possibility of antenna designs other than loop-shape in future.

5 Acknowledgements

Present study is the result of "Development of laser remote analysis for next generation nuclear fuel and applied study by MOX sample" entrusted to Japan Atomic Energy Agency by

the Ministry of Eduction, Culture, Sports, Science, and Technology of Japan (MEXT).

Notes and references

1 J. P. Singh, F. Y. Yueh, H.Zhang and K. Carney, *Recent.Res.Devel.Applied Spectroscopy*, 1999, **2**, 59–67.

2 P. Fichet, P. Mauchien and C. Moulin, *Applied Spectroscopy*, 1999, **53**, 1111–1117.

3 L. St-Onge, M. Sabsabi and P. Cielo, *Spectrochim. Acta B*, 1998, **53**, 407–415.

4 V. Babushok, F. D. Jr, J. Gottfried and C. M. A. Miziolek, *Spectrochim. Acta B*, 2006, **61**, 999–1014.

5 F. Colaoa, V. Lazica, R. Fantonia and S. Pershinb, *Spectrochim. Acta B*, 2002, **57**, 1167–1179.

6 M. Oba, Y. Maruyama, K. Akaoka, M. Miyabe and I. Wakaida, *Appl. Phys. A: Mater. Sci. Process.*, 2010, **101**, 545.

7 R. Coons, S. Harilal, S. Hassan and A. Hassanein, *Appl. Phys. B.*, 2012, **107**, 873–880.

8 W. Sdorra, A. Quentmeier and K. Niemax, *Mikrochim Acta II*, 1989, **2**, 201.

9 I. B. Gornushkin, S. A. Baker, B. W. Smith and J. D. Winefordner, *Spectrochim. Acta B*, 1997, **52**, 1653.

10 F. H. Kortenbruck, R. Noll, P. Wintjens, H. Falk and C. Becker, *Spectrochim. Acta B*, 2001, **56**, 933.

11 S. L. Lui, Y. Godwal, M. T. Taschuk, Y. Y. Tsui and R. Fedosejevs, *Anal. Chem*, 2008, **80**, 1995.

12 S. Laville, C. Goueguel, H. Loudyi, F. Vidal, M. Chaker and M. Sabsabi, *Spectrochim. Acta B*, 2009, **64**, 347.

13 H. Loudyi, K. Rifai, S. Laville, F. Vidal and M. C. andM. Sabsabi, *J. Anal. At. Spectrom.*, 2009, **24**, 1421.

14 X. K. Shen, H. Wang, Z. Q. Xie, Y. Gao, H. Ling and Y. F.Lu, *Appl. Opt.*, 2009, **48**, 2551.

15 D. Cleveland, P. S. X. Hou, K. X. Yang, J. Zhou and R. G. Michel, *Appl. Spectrosc.*, 2005, **59**, 1427.

16 S. L. Lui and N. H. Cheung, *Anal. Chem.*, 2005, **77**, 2617.

17 C. Goueguel, S. Laville, F. Vidal, M. Sabsabi and M. Chaker, *J. Anal. At. Spectrom*, 2010, **25**, 635.

18 D. Cleveland and R. G. Michel, *Microchem. J.*, 2010, **95**, 120.

19 C. Goueguel, S. Laville, F. Vidal, M. Chaker and M. Sabsabi, *J. Anal. At. Spectrom.*, 2011, **26**, 230.

20 K. Rifai, F. Vidal, M. Chaker and M. Sabsabi, *J. Anal. At. Spectrom*, 2013, **28**, 388.

21 O. A. Nassef and H. E. Elsayed-Ali, *Spectrochim. Acta, Part B*, 2005, **60**, 1564–1572.

22 K. Li, W. Zhou, Q. Shen, J. Shao and H. Qian, *Spectrochim. Acta, Part B*, 2010, **65**, 420–424.

23 W. Zhou, K. Li, Q. Shen, Q. Chen and J. Long, *Opt. Express*, 2010, **18**, 2573–2578.

24 W. Zhou, X. Su, H. Qian, K. Li, X. Li, Y. Yu and Z. Ren, *J. Anal. At. Spectrom.*, 2013, **28**, 702–710.

25 K. Tereszchuk, J. Vadillo and J. Laserna, *J. Anal. At. Spectrom.*, 2007, **22**, 183–186.

26 K. Tereszchuk, J. Vadillo and J. Laserna, *Appl. Spectrosc.*, 2008, **62**, 1262–1267.

27 K. Tereszchuk, J. Vadillo and J. Laserna, *Spectrochim. Acta B*, 2009, **64**, 378–383.

28 J. Uebbing, A. Ciocan and K. Niemax, *Spectrochim. Acta B*, 1992, **47**, 601–610.

29 Y. Liu, M. Baudelet and M. Richardson, *J. Anal. At. Spectrom*, 2010, **25**, 1316–1323.

30 Y. Liu, B. Bousquet, M. Baudelet and M. Richardson, *Spectrochim. Acta B*, 2012, **73**, 89–92.

31 Y.Ikeda and R. Tsuruoka, *Applied Optics*, 2012, **51**, B183–B191.

32 K.T.Macdonald, http://www.physics.princeton.edu/ mcdonald/examples/smallloop.pdf.

33 http://www.cfa.harvard.edu/amp/ampdata/kurucz23/sekur.html

34 W. Sdorra, J. Brust and K. Niemax, *Mikrochim Acta*, 1992, **108**, 1–10.

35 A. H. El-Astal, S. Ikram, T. Morrow, W. G. Graham and D. G. Walmsley, *J. Appl. Phys*, 1995, **77**, 6572–6580.

36 J. A. Aguilera and C. Aragon, *Spectrochim. Acta B*, 2008, **63**, 784–792.

37 S. S. Harilal, B. OfShay and M. S. Tillack, *J. Appl. Phys.*, 2005, **98**, 013306.

38 M.Miyabe, M.Oba, H.Iimura, K.Akaoka, Y.Maruyama and I.Wakaida, *Appl Phys A*, 2010, **101**, 65–70.